Spin−Orbit Coupling Effect and Intramolecular Orbital Interactions: Penning Ionization of CH_2BrCl, $CHBrCl_2$, and CH_2BrCN by Collision with He*(2^3S) Metastable Atoms

Shan Xi Tian, Naoki Kishimoto, and Koichi Ohno*

Department of Chemistry, Graduate School of Science, Tohoku University, Aramaki, Aoba-ku, Sendai 980-8578, Japan

Received: August 19, 2002; In Final Form: January 13, 2003

He*(2^3S) Penning ionization electron spectra (PIES) as well as He I ultraviolet photoelectron spectra have been measured for CH_2BrCl, $CHBrCl_2$, and CH_2BrCN. For the lower ionization-potential bands, spin−orbit split states are assigned in the spectra for CH_2BrCl and CH_2BrCN, whereas valence-orbital, ionic states are assigned for $CHBrCl_2$. These assignments are based on the fact that the intramolecular orbital interactions in $CHBrCl_2$ are much stronger than those in the other molecules, whereas the spin−orbit coupling effects predominate for the other two molecules. Collision energy dependence of partial Penning ionization cross sections and the PIES indicate that the magnitudes of the attractive interactions in the electron distribution regions of the lone pair orbitals (n) of the Cl and Br atoms and the N atom in the CN group and π_{CN} orbitals are in a sequence of $n_N \gg n_{Br} \sim \pi_{CN} > n_{Cl}$.

I. Introduction

A molecule M can be ionized by collision with a metastable atom A* having an excitation energy larger than the lowest ionization potential (IP) of the molecule; this process is known as Penning ionization.[1] Experimental studies on Penning ionization can be worked out by different measurements such as kinetic energy (E_e) of the electrons emitted, collision energy (E_c) dependence of total or partial ionization cross sections, and the electron energy spectra in coincidence with the specific ion produced.

Penning ionization electron spectra (PIES) can be obtained by measuring the E_e values.[2] Spectral characteristics of PIES have been noted in comparison with He I ultraviolet photoelectron spectra (UPS) since the pioneering work by Čermák:[2,3] (i) A peak shift (ΔE) is frequently observed in PIES with respect to the corresponding UPS. (ii) Band shapes in PIES show somewhat broader features. (iii) Band intensities in PIES are different from those in UPS. Two fundamental models have been suggested for interpreting these characteristics: (a) a two-state (incoming and outgoing channels) potential curve model proposed by Hermann and Čermák[4] and (b) the electron exchange model suggested by Hotop and Niehaus.[5] If we assume that the potential curve of the outgoing channel is rather flat for the Penning ionization involving metastable rare gas atoms, the peak shift ΔE is approximately related to the incoming potential curve.[6] In the exchange mechanism, the ionization occurs mainly at the turning point through a transfer of an outer-orbital electron of M into the inner-orbital vacancy of A*, which in turn ejects the external electron.[5] The band intensities are closely related to an overlap between the wave functions of a certain molecular orbital (MO) and one of the inner atomic orbitals of A*, reflecting the respective orbital reactivity for Penning ionization. On the basis of this approximation, the relative intensity of bands in PIES can be successfully compared with the exterior electron density (EED) for individual MOs, where the EED value is a measure of how far electron distributions expand outside a molecular boundary.[7] Furthermore, anisotropy effects are expected to be significant in Penning ionization of molecules. On the basis of the above theoretical view, one can understand easily the fact that an A* approach along a given direction can lead to a preferential ejection of the electron from a specific MO characterized by an electron density distribution extended toward the incoming A*.[7] Therefore, the anisotropy of an MO electron density distribution can be reflected in Penning ionization dynamics. Thereby, the partial ionization cross sections should depend on the relative velocity (or collision energy, E_c) between A* and M.

The coupled techniques including velocity selection (collision-energy-resolved) and electron kinetic energy analysis have been developed.[8−10] Velocity-controlled supersonic metastable beams have been utilized to measure collision-energy-resolved PIES (CERPIES) by collision with He*(2^1S,2^3S).[11] In our laboratory, the cross-correlation time-of-flight (TOF) method together with a pseudorandom chopper is utilized to measure the velocity distribution of A* and the time-dependent distribution of Penning electrons.[12] We can measure two-dimensional (electron-energy and collision-energy-resolved) PIES (2D-PIES) efficiently, where collision energy dependence of partial ionization cross sections (CEDPICS) can also be obtained simultaneously by measuring CERPIES.[13] Therefore, we can get information of anisotropic interactions of the steric access of A* to M. Typically, a negative CEDPICS accompanied by a negative ΔE shows that there is an attractive region for a certain MO; a positive CEDPICS accompanied by a positive ΔE shows a repulsive case.

Recently, a series of CERPIES and CEDPICS studies have been reported for specific molecules having a cyano (CN) group (CH_3SCN,[14] CH_3CN,[15] C_3H_5CN,[16] NCCN,[17] CH_3CH_2CN,[12] CH_2CHCN,[12] CH_2CHCH_2CN[12]). These results indicate that the interaction potentials between He*(2^3S) and π_{CN} orbitals are strongly attractive around the cyano group. In particular, an interesting conjugation effect was observed for CH_2CHCN in a comparison with CH_2CHCH_2CN.[12] On the other hand, halohydrocarbons also attracted our interest because the lone pair orbitals (n) of halogen atoms show distinctly attractive interac-

10.1021/jp0218950 CCC: $25.00
Published on Web 03/12/2003

tions. It has been found that perpendicular approach of the He*(2^3S) atom with respect to the C−Cl (or Br, I) bond axis is more attractive than approaches in the other directions,[18−21] whereas the approach along the C−F bond axis is more attractive for fluorohydrocarbons.[19,20] Moreover, the most attractive interactions in two perpendicular directions with respect to the C−Cl (or Br, I) bond axis may be slightly changed in some molecules, such an effect can be obtained from the model potential curves.[22,23] However, these differences, reflecting the interaction anisotropy, cannot be exhibited by CEDPICS when the intramolecular orbital interactions are too weak to compete with the strong spin−orbit (SO) coupling effects. Namely, the CEDPICS for the SO split bands are almost equal. As interpreted previously,[23] although the lone pair electrons of the halogen atom are in two different orbitals (in a C_s symmetry molecule), they are still energetically degenerate if the intramolecular orbital interaction (or localized molecular interaction field) is extremely weak. These two orbitals having four electrons can be approximated as one orbital, and the total angular momentum of the electrons is crudely approximated to be a good quantum number. The SO coupling effect leads to two degenerate ionic states $^2E_{1/2}$, and two ionization bands will be observed. For these two SO split bands, the electron energy spectra only supply us with the energetic information on these two states, which cannot directly correspond to the spatial electron distributions of the related two MOs. Thereby, the interaction anisotropy arising from the different spatial electron distributions cannot be reflected by CEDPICS for the SO split bands.

On the other hand, a strongly attractive interaction is usually caused by an electron-transfer process in which the target molecule acts as an electron acceptor.[12,24] Thereby, the magnitudes of attractive interactions around halogen atoms and a cyano group are closely related to their electron affinity (EA). As the cyano radical has a remarkable EA value (3.82 eV)[25] much higher than the halogens ($EA_F = 1.7$ eV, $EA_{Cl} = 1.81$ eV, $EA_{Br} = 1.69$ eV),[26] a competition between halogen anion and cyano anion formation is expected to happen when an additional electron is attached to a pseudobihalogen molecule XCN (X = F, Cl, Br, and I)[27] or a haloacetonitrile (CH_2XCN).[28] Dissociative detachment has been observed for the haloacetonitriles using flowing-afterglow mass spectrometry.[28] Recently, the 2D-PIES and emission spectrum of CN($B^2\Sigma^+$) fragment produced by the He*(2^3S)-collision dissociation were studied for BrCN.[29a] Some particular dissociation processes were found to be involved in the collisions with the metastable atoms.[29] On the other hand, halogenated derivatives of methane have received continuous interest from Novak and co-workers,[30−32] in which the intramolecular orbital (n ↔ n and n ↔ σ) interactions were studied by the measurements of He I and He II UPS,[30,32] and angle-resolved photoelectron spectra using the synchrotron radiation.[31] In particular, two lowest-ionization-potential ionic states (the corresponding orbitals $7b_2$ and $3b_1$ having the n_{Cl} characteristics) in the UPS of CH_2Cl_2[33] split into two distinctly separated bands in the UPS of $CHBrCl_2$,[32] whereas the other n_{Cl} bands cannot be resolved clearly in the UPS both of $CHBrCl_2$[32] and of CH_2Cl_2.[33] These results may be interpreted not only by the different molecular symmetries but also by the existence of the Br atom in $CHBrCl_2$, which can lead to stronger intramolecular orbital n_{Cl} ↔ n_{Cl} and n_{Cl} ↔ n_{Br} interactions. To our best knowledge, no similar studies are extended to CH_2-XCN for studying the orbital n_X ↔ π_{CN} interactions.

As mentioned above, the 2D-PIES measurements have a considerable stereochemical significance for elucidation of MO characteristics, in particular, CEDPICS further provides insight into anisotropic interactions and the role of the electrophilic reactions by exhibiting distinctly different slopes for the related bands (or orbitals). Regarding the spectral assignments, there is a paradox on the SO split bands, particularly for the low symmetry molecules having halogen atoms. Even for the strong SO coupling effect (e.g., Br atom), it is somehow unclear that we should use the SO split states or ionic states of respective MOs for the assignments of the split n_{Br} bands when the intramolecular orbital interactions compete with the SO coupling effects. Although the n_{Br} MOs (a′ and a″ for the C_s symmetry molecule) exhibit the specifically spatial distributions of electron densities, it is meaningful to investigate whether 2D-PIES can derive this information by showing the different slopes of CEDPICS. It is also interesting to investigate the orbital reactivity for the n_{Cl}, n_{Br}, n_N (in the CN group), and π_{CN} orbitals shown in Penning ionizations by collision with the He*(2^3S) atoms. In this study, CH_2BrCl, $CHBrCl_2$, and CH_2BrCN are studied by the 2D-PIES technique as well as theoretical calculations.

II. Experimental Method

The experimental apparatus used in this study has been reported elsewhere.[8−10,12,13] Metastable atoms of He*(2^3S) were produced by a discharged nozzle source with a tantalum hollow cathode. He I resonance photons (584 Å, 21.22 eV) produced by a discharge in pure helium gas were used to obtain UPS. The kinetic energies of the electrons ejected in Penning ionization or photoionization were determined by a hemispherical electrostatic deflection type analyzer using an electron collection angle 90° to the incident He* beam axis or He I photon beam axis. The energy resolution of the electron analyzer was estimated to be 80 meV from the full width at half-maximum (fwhm) of the $Ar^+(^2P_{3/2})$ peak in the He I UPS for the higher-energy-resolution PIES and UPS measurements of the samples; for the CEDPICS measurements, the resolution was lowered to 250 meV to obtain higher electron counting rates. The transmission efficiency curves of the electron energy analyzer for both of these two modes were determined by comparing our UPS data of some molecules with those obtained by Kimura et al.[33] and Gardner and Samson.[34]

For the collision-energy-resolved measurements of Penning ionization, the metastable He*(2^3S) beam was modulated by a pseudorandom chopper, and then introduced into a reaction cell. Time dependent electron signals for each kinetic electron energy E_e were recorded with scanning electron energies of a 40 meV step and the dwell time for the TOF measurements was 3 μs. The CEDPICS were obtained from 2D data within an appropriate range of E_e (typically the fwhm of the respective band) to avoid the effect of neighboring bands. The CEDPIES were cut at the two E_c (110 and 250 meV) from 2D data with some width.

The volatility at room temperature is high enough to create a sufficient concentration of target molecules in the gas phase, and the ambient pressure was controlled at ca. 2×10^{-5} Torr.

III. Calculations

The geometrical parameters of these three molecules were optimized with C_s symmetry using the second-order Møller−Plesset perturbation (MP2) method and 6-311+G(d,p) basis set. To obtain the MO wave functions, Hartree−Fock self-consistent-field (HF−SCF) calculations with the 6-311+G(d,p) basis were performed over the optimized structures. Electron density contour maps for respective SCF MOs are plotted, where thick solid curves indicate the repulsive molecular surface ap-

proximated by atomic spheres of van der Waals radii (r_C = 1.7 Å, r_H = 1.2 Å, r_{Cl} = 1.8 Å, r_{Br} = 1.95 Å, r_N = 1.5 Å).[35] The IP values were calculated by the outer valence Green's function (OVGF) method[36] with the 6-311+G(d,p) basis set.

It is well-known that the shape of velocity dependence of the total scattering cross section of He*(2^3S) by He, Ar, and Kr is very similar to that of Li(2^2S),[37a] and interaction well depths and locations of potential wells have been found to be very similar for interactions of various targets with He*(2^3S) and Li(2^2S).[5,37b,c] So this similarity between He*(2^3S) and Li(2^2S) is usually used to compare the computationally much more feasible Li−M potentials with the experimental results on the He*(2^3S)−M interactions.[13−24,29a] In this study, the interaction potential calculations with the Li(2^2S) atom, $V^*(R,\theta,\phi)$ (where R, θ, and ϕ were defined in the figures), were performed at the unrestricted MP2 level of theory using the 6-31+G(d,p) basis set with scanning R, θ, or ϕ values and the geometrical parameters of the targets fixed at the previously optimized values. Spin contamination is negligible for these calculations. The present calculations of interaction potentials and IP values were performed with GAUSSIAN 98.[38]

IV. Results

The He I UPS and He*(2^3S) PIES of CH_2BrCl, $CHBrCl_2$, and CH_2BrCN are shown in Figures 1−3, respectively. SO in the assignments represents the spin−orbit coupling effect. S* bands in the PIES of Figures 1 and 2 represent the autoionization band, whereas S(S*) represents the possibility of satellite states mixed with autoionizations. The details will be discussed in section V.

Figures 4−6 show the CERPIES of CH_2BrCl, $CHBrCl_2$, and CH_2BrCN, respectively. Hot spectra at the higher E_c ca. 250 meV are exhibited by dotted curves, and cold spectra at the lower E_c ca. 110 meV are exhibited by solid curves.

log σ vs log E_c plots of the CEDPICS in a collision energy range of 100−300 meV are shown in Figures 7−9 for CH_2BrCl, $CHBrCl_2$, and CH_2BrCN, respectively. The calculated electron density maps are given to grasp the most effective directions of the ionization or effective access of the He* atom. The maps having the molecular surfaces represented by the thinner curves, for a″-type orbitals of CH_2BrCl and CH_2BrCN, were plotted on a plane 1.7 Å (van der Waals radius of C atom) above the molecular nodal plane. SO in the figures indicated that two bands are separated by the strong SO coupling effect. The schematic diagrams of the MOs of $CHBrCl_2$ are shown in Figure 8 for clearly representing the MO characteristics, where the solid circles showed a valence s orbital, and couples of ellipses and dashed circles show in-plane and out-of-plane components of p orbitals.

Figures 10−13 show the calculated interaction potential energy curves for these three molecules. For a comparison of anisotropic interactions of the n_{Cl} and n_{Br} orbitals in the different molecules, the interaction energies were calculated in the directions perpendicular to each other in the certain planes including the C−Cl or C−Br bond. Moreover, we scanned the polar angle θ and the azimuthal angle ϕ in two planes perpendicular to each other for $CHBrCl_2$.

Tables 1−3 summarized the experimental and calculated IPs, experimental peak shifts ΔE, slope parameters (m) of CEDPICS, and the band assignments with the orbital characteristics. The slope parameters were obtained by a least-squares fitting of the log σ vs log E_c plots in a collision energy range of 100−300 meV. The vertical IPs were determined from present He I UPS except for some specific notations. The ΔE values were obtained as the differences between the peak positions in PIES (E_{PIES}, in electron energy scale) and the nominal value (E_0, difference between the metastable excitation energy and sample IP), $\Delta E = E_{PIES} - E_0$.

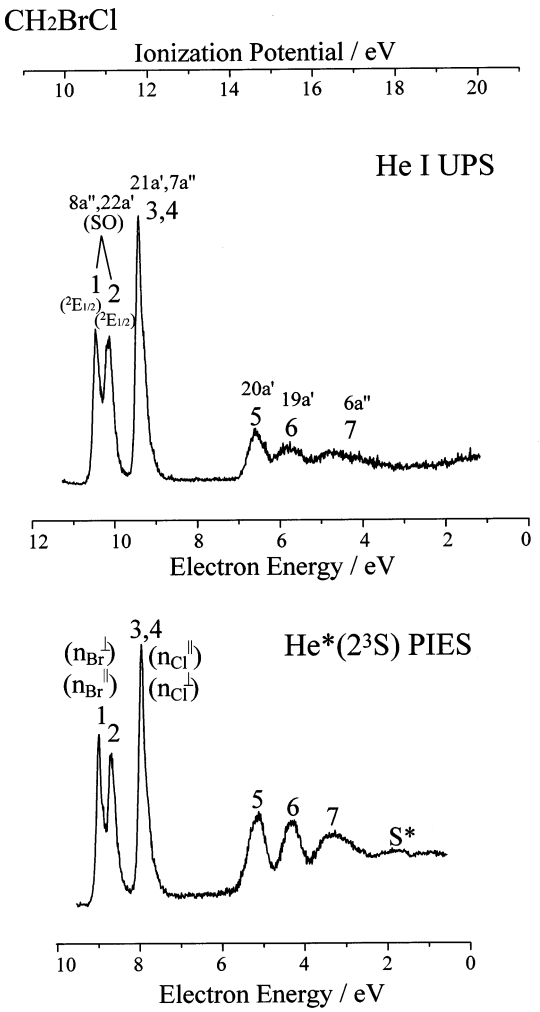

Figure 1. He I UPS and He*(2^3S) PIES of CH_2BrCl. SO represents the strong spin−orbit coupling effect.

V. Discussion

A. Features in PIES and UPS. The He I UPS of these molecules except for CH_2BrCN have been reported.[31] In particular, the extensive assignments in the He I and He II UPS have been made by Novak et al. not only for CH_2BrCl and $CHBrCl_2$ but also for other halogenated methanes.[30−32,39] However, some arguments on the assignments should be addressed here. As discussed in one of our previous reports,[23] the SO split bands cannot simply be assigned by normal ionic states of respective MOs. If a strong SO coupling effect plays a crucial role in the band splitting, the ionic states for the split bands should be assigned ($^2E_{1/2}$ for the C_s symmetry molecules) using the extended group suggested by Herzberg et al.[40] On the contrary, the assignments of normal ionic states can be used when the intramolecular orbital through-space (or through-bond) interaction and hyperconjugation predominate. To judge whether an SO coupling effect is relatively important is based on the split energies of two bands, on the band shapes, and CEDPICS. The band shape can reflect the interactions between the n electrons and the electrons of other groups or bonds, usually by exhibiting vibrational structures. CEDPICS accurately indicates whether two split bands correspond to two different MOs

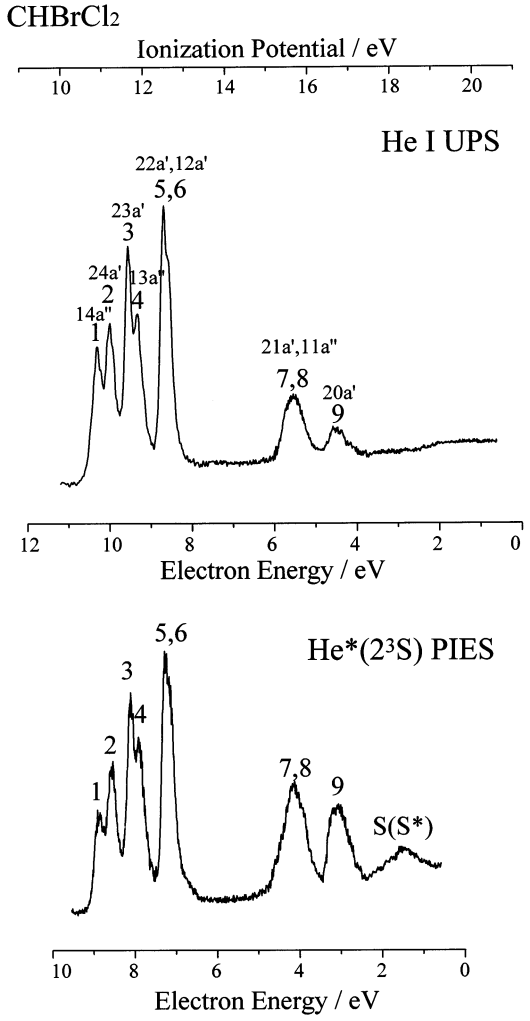

Figure 2. He I UPS and He*(2^3S) PIES of $CHBrCl_2$.

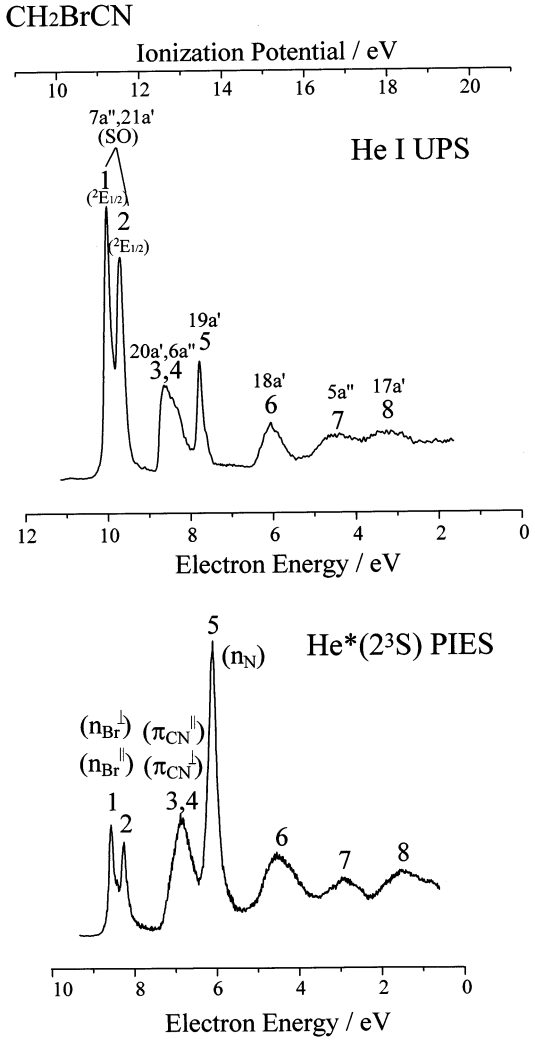

Figure 3. He I UPS and He*(2^3S) PIES of CH_2BrCN. SO represents the strong spin−orbit coupling effect.

respectively or have a mixed characteristic of two MOs. The anisotropic interactions can be reflected by the distinctly different slopes of CEDPICS for the bands corresponding to the MOs having different spatial electron distributions, but they cannot be reflected (and show almost identical slopes) for the bands corresponding to the mixed MO characteristics.[23,42] Therefore, the normal ionic states can be assigned for the former, but the SO coupling splits states for the latter. Because the effects of energy-level[21,43] and the MO electron density distributions[12,14−16,18−23,42b] can be reflected by CEDPICS, the slope of CEDPICS is the most important of the three techniques to determine characteristics of the split bands. In Figures 1 and 3, bands 1 and 2 exhibit different band shapes. Vibrational structures have been recognized in the high-energy-resolution UPS for these bands.[32] However, the strong SO coupling effects of the Br atoms are still the most important factor because these two bands have the typical characteristics caused by SO coupling: the first band has a little higher intensity with respect to the second band both in He I UPS and in He*(2^3S) PIES[42a] (also see Figures 1 and 3), and these two bands have similar CEDPICS[23,42b] (as discussed in section B). Nonetheless, it is surprising that band 1 is weaker than band 2 for $CHBrCl_2$ in Figure 2. A strong intramolecular orbital interaction is expected in this molecule. As is well-known, the OVGF method cannot predict the SO splitting energy,[36] but the IP values of bands 1 and 2 have been well predicted only for $CHBrCl_2$. This result indicates that these bands have characteristics of ionic states of respective MOs. Therefore, the SO split bands 1 and 2 are assigned with two $^2E_{1/2}$ ionic states for CH_2BrCl and CH_2BrCN rather than $CHBrCl_2$.

The orbital assignments used in this work are numbered from the core orbital for each molecule, which differs from the assignments given by Novak et al.[30−32] In Figure 1, the relative intensities of bands 1−4 in the UPS are similar to those in the PIES. This result contrasts to bands 1−5 in Figure 3, where bands 3−5 are enhanced significantly with respect to bands 1−2 in the PIES. As mentioned in the Introduction, the band intensities in PIES are closely related to the EED values of the respective MOs, further reflecting the orbital reactivity in Penning ionization. Regarding the MO characteristics of bands 1−5 in Figures 1 and 3 (see electron density maps in Figures 7 and 9), a reactivity sequence in Penning ionizations for the n_{Cl}, n_{Br}, n_N, and π_{CN} orbitals can be estimated by the relative ratios of band intensities in the PIES, n_N (ca. 1.8) > π_{CN} (ca. 1.6) > n_{Br} (ca. 1.4) > n_{Cl} (ca. 1.0). Here some arguments should be addressed for bands 3 and 4 (20a′, $\pi_{CN}^{||}$, the parallel distribution, and 6a″, $\pi_{CN}^{\perp}$, the perpendicular distribution). In a high symmetry (e.g., C_{3v}), the SO coupling effect together with Jahn−Teller effect leads to the split bands for a degenerate π_{CN} orbital. In CH_2BrCN, the lower C_s symmetry results in a large splitting energy ca. 200 meV estimated by the OVGF calculations in Table 3. Moreover, one may notice the great band-shape changes in a comparison between the UPS and PIES

TABLE 1: Band Assignments, Ionization Potentials (IP, eV), Peak Shifts (ΔE, meV), and Slope Parameters (m) for CH_2BrCl

band	IP_{obsd}	IP_{OVGF} (pole strength)	orbital character	ΔE	m
1[a]	10.75	10.62 (0.94)	8a″($n_{Br}^{\perp}$)	−80 ± 10	−0.35
2[a]	11.08	10.65 (0.94)	22a′($n_{Br}^{\parallel}$)	−50 ± 20	−0.36
3	11.79	11.43 (0.92)	21a″($n_{Cl}^{\parallel}$)	−60 ± 10	−0.31
4		11.50 (0.92)	7a″($n_{Cl}^{\perp}$)		
5	14.63	14.40 (0.92)	20a′(σ_{CBr})	−20 ±20	−0.21
6	15.40	15.28 (0.91)	19a′(σ_{CCl}, σ_{CH})	−10 ± 40	−0.22
7	16.32	16.59 (0.90)	6a″(π_{CH})	−10 ± 80	−0.19
S*	17.9−18.2[b]				−0.16

[a] Spin−orbit split bands (details discussed in text). [b] Estimated from the PIES in Figures 1 and 4.

TABLE 2: Band Assignments, Ionization Potentials (IP, eV), Peak Shifts (ΔE, meV), and Slope Parameters (m) for $CHBrCl_2$

band	IP_{obsd}	IP_{OVGF} (pole strength)	orbital character	ΔE	m
1	10.91	10.85 (0.92)	14a″($n_{Br}^{\parallel}$, σ_{CCl})	−70 ± 20	−0.32
2	11.21	11.09 (0.92)	24a′($n_{Br}^{\perp}$, σ_{CH}, σ_{CCl})	−60 ± 20	−0.35
3	11.65	11.48 (0.92)	23a′($n_{Cl}^{\perp}$, $n_{Br}^{\perp}$)	−60 ± 10	−0.30
4	11.88	11.65 (0.91)	13a″($n_{Cl}^{\parallel}$, $n_{Br}^{\parallel}$)	−20 ± 10	−0.31
5	12.52	12.31 (0.91)	22a′ ($n_{Cl}^{\perp}$, $n_{Br}^{\perp}$)	−50 ± 20	−0.33
6		12.34 (0.90)	12a″(π_{CCl})		
7	15.62	15.35 (0.90)	21a′(σ_{CH}, σ_{CCl})	0 ± 60	−0.23
8		15.69 (0.90)	11a″(σ_{CCl})		
9	16.65	16.67 (0.90)	20a′(σ_{CH}, C_{2s}, Cl_{3s})	−20 ± 60	−0.23
S(S*)	18.0−18.3[a]				−0.19

[a] Estimated from the PIES in Figures 2 and 5.

TABLE 3: Band Assignments, Ionization Potentials (IP, eV), Peak Shifts (ΔE, neV), and Slope Parameters (m) for CH_2BrCN

band	IP_{obsd}	IP_{OVGF} (pole strength)	orbital character	ΔE	m
1[a]	11.21	10.97 (0.94)	7a″($n_{Br}^{\perp}$)	−40 ± 0	−0.34
2[a]	11.52	11.04 (0.94)	21a′($n_{Br}^{\parallel}$)	−50 ± 10	−0.35
3	12.57[b]	12.34 (0.91)	20a′($\pi_{CN}^{\parallel}$)	−190 ± 60[c]	−0.35
4		12.54 (0.91)	6a″($\pi_{CN}^{\perp}$)		
5	13.44	13.97 (0.90	19a′(n_N)	−290 ± 20	−0.46
6	15.10	14.49 (0.91)	18a′(σ_{CN}, σ_{CBr})	−40 ± 80	−0.36
7	16.95[d]	16.96 (0.91)	5a″(π_{CH})	−20 ± 100	−0.23
8	18.20[d]		17a′(σ_{CH})		−0.20

[a] Spin−orbit split bands (details discussed in text). [b] The approximately adiabatic IP value in the UPS of Figure 3. [c] Estimated between band 3 (in UPS) and band 4 (in PIES). [d] Estimated with a big experimental error (ca. 0.10 eV).

for the overlap band 3 and 4 in Figure 3. It seems that the magnitude of enhancement for band 4 (6a″, $\pi_{CN}^{\perp}$) should be larger than band 3 (20a′, $\pi_{CN}^{\parallel}$) in the PIES. This difference as well as the large splitting energy indicates that these two bands correspond to ionization from two MOs rather than the SO split states. The interpretation to this difference is that the approaches perpendicular to the molecular nodal plane (for 6a″, $\pi_{CN}^{\perp}$) are more effective than the in-plane approaches (for 20a′, $\pi_{CN}^{\parallel}$). Similarly, this can explain the observation in which band 2 is much stronger than band 1 in the PIES of Figure 2. These shielding effects by the hindrance of the repulsive interactions along C−Cl and C−Br bond axes will be discussed in detail in section B. Moreover, band 7 in the PIES of Figure 3 is relatively weak due to the repulsive interaction around the CH_2 group (see Figure 10a), although the π_{CH} electrons are distributed extensively. However, a distinguished enhancement of band 5 in Figure 3 cannot be explained by the extensive electron distribution of the corresponding MO 19a′(n_N), it is owed to

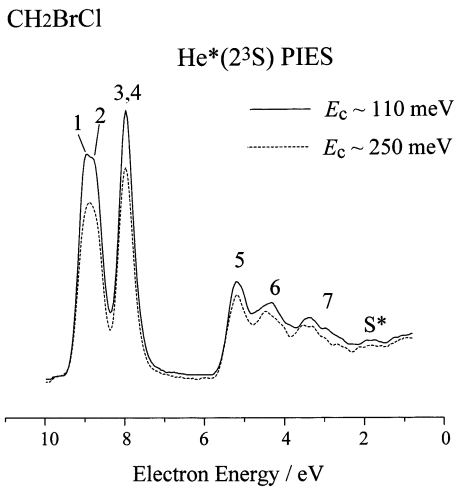

Figure 4. Collision-energy-resolved He*(2^3S) PIES of CH_2BrCl: solid curve, $E_c \sim 105-115$ meV, average 110 meV; dotted curve, $E_c \sim 237-263$ meV, average 250 meV.

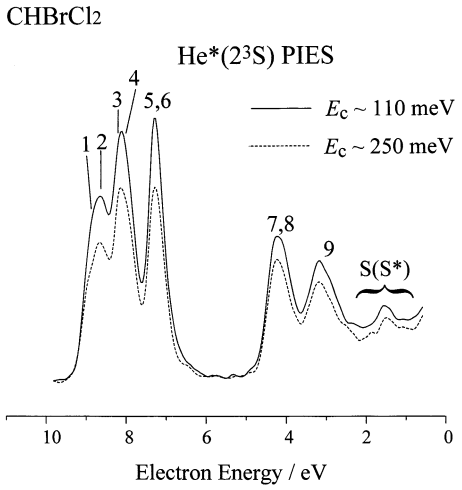

Figure 5. Collision-energy-resolved He*(2^3S) PIES of $CHBrCl_2$: solid curve, $E_c \sim 106-114$ meV, average 110 meV; dotted curve, $E_c \sim 238-262$ meV, average 250 meV.

strong attraction for the He* access along the CN axis. This phenomenon was observed in CERPIES of nitrile compounds.[12,14−17] Band 9 in Figure 2 is enhanced significantly in the PIES with respect to that in the UPS because the corresponding 20a′ orbital has some characteristics of C_{2s} orbital (see Figure 8), and it has been noted that the resonant excitation transfer and the subsequent autoionization frequently occurs for the C_{2s} bands.[10]

The S* and S(S*) bands have been observed clearly in the PIES of Figures 1, 2, 4, and 5. They may not belong to the satellite states related to shake-up or shake-off processes, because no similar bands were observed at the same energy regions in the photoelectron spectra by the synchrotron radiation[31] and He II radiation.[32] On the other hand, the photoexcitation and photodissociation dynamics of CH_2BrCl have been investigated both theoretically[44] and experimentally.[45] Two dissociative products, Cl and Br, were expected to predominate in the energetically favored channels.[45] The relationship between ionization and formation of Rydberg states has been pointed out by Miller and Morgner.[46] In the PIES, the autoionizations of Rydberg-state atomic fragments as the dissociative products in Penning ionization were frequently observed.[47,48] The series lines of autoionizations usually become a broad flat band in the electron low-energy-resolution spectra.[47e,48] Therefore, the

TABLE 4: Excitation Energies and Dissociation Energies with Respect to the Neutral Ground-State CH_2BrCl

transition	energy (eV)
Excitation (Theoretical)[a]	
$n_{xBr} \rightarrow \sigma^*_{(CBr)}$	6.12
$n_{yBr} \rightarrow \sigma^*_{(CBr)}$	6.04
$n_{zCl} \rightarrow \sigma^*_{(CCl)}$	7.18
$n_{xBr} \rightarrow$ Rydb A′	7.42
$n_{yBr} \rightarrow$ Rydb A′	7.40
$n_{zCl} \rightarrow$ Rydb A′	8.15
$n_{xBr} \rightarrow \sigma^*_{(CCl)}$	8.59
$n_{yBr} \rightarrow$ Rydb A″	9.09
$n_{xBr} \rightarrow$ Rydb A″	9.16
Excitation (Experimental)	
$n_{Br} \rightarrow \sigma^*_{(CBr)}$	6.1 (202.6 ± 0.5 nm)[b] (203 nm)[c]
$n_{Cl} \rightarrow \sigma^*_{(CCl)}$	7.17 (173 nm)[d]
	7.56 (164 nm)[e]
$n_{zCl} \rightarrow \sigma^*_{(CBr)}$	7.8[d]
Dissociation	
$CH_2Cl + Br$	2.95 (285 kJ/mol)[f]
$CH_2Br + Cl$	3.43 (331 kJ/mol)[f]

[a] From ref 46, calculated at the MS-CASPT2 level. The transitions having oscillator strengths larger than 0.007 are listed in this table. [b] From ref 45g. [c] From ref 45d. [d] Estimated by Rozgonyi et al., in ref 44. [e] Estimated by Lee et al., in ref 45c, and used in ref 45e. [f] From ref 45f.

S* band in Figure 1 may indicate autoionizations of Cl** or Br** species, whereas S(S*) in Figure 2 may comprise a mixed band of some satellite states and the autoionizations because its band shape differs from the S* band. Here the PIES of CH_2BrCl is analyzed as an example. Table 4 summarizes the related excitation and formation energies available from the literature.[44,46] In general, the following processes may be involved in the Penning ionizations:

$$\begin{aligned} He^*(2^3S) + CH_2BrCl &\rightarrow He + CH_2BrCl^* \\ &\quad \text{(valence-excited or Rydberg states)} \\ &\rightarrow He + CH_2Br + Cl^{**} \qquad (1) \\ &\rightarrow He + CH_2Cl + Br^{**} \end{aligned}$$

then followed by the autoionizations $Cl^{**} \rightarrow Cl^+ + e^-$ and $Br^{**} \rightarrow Br^+ + e^-$. As shown in Table 4, the excitation energies for the molecular Rydberg states are smaller than the ionization potentials of the n_{Cl} and n_{Br} orbitals but are much higher than the dissociation energies. If $n_{Cl} \rightarrow \sigma^*_{CCl}$ and $n_{Br} \rightarrow \sigma^*_{CBr}$ are involved, the dissociation energy barrier of the excited CH_2BrCl will be lowered because the excited electron occupies an antibonding σ^*_{CCl} or σ^*_{CBr} orbital. Therefore, the excitation transfer may be energetically favored with respect to the ionization−dissociation processes. Similar processes are expected to occur for $CHBrCl_2$. In the PIES of Figures 1 and 2, bands S* and S(S*) are structureless due to the energy resolution (ca. 80 meV). Although there are no clear bands corresponding to the above processes observed in the PIES for CH_2BrCN because the valence-orbital-ionization band 7 is just in that energy region (see Figure 3), the autoionizations of Br** atom cannot be excluded. However, the excited CN species dissociated from CH_2BrCN by the He* collision should be rare.[29b] Moreover, we cannot determine which autoionization process ($Cl^{**} \rightarrow Cl^+ + e^-$ or $Br^{**} \rightarrow Br^+ + e^-$) plays a more important role for band S*. The branching ratio of C−Cl and C−Br bond cleavage was observed to be dependent on the photon energies, but the C−Br bond cleavage was predominate.[45] The double

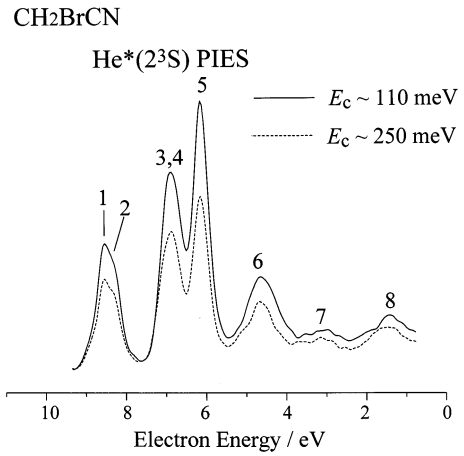

Figure 6. Collision-energy-resolved He*(2^3S) PIES of CH_2BrCN: solid curve, $E_c \sim 107-113$ meV, average 110 meV; dotted curve, $E_c \sim 241-259$ meV, average 250 meV.

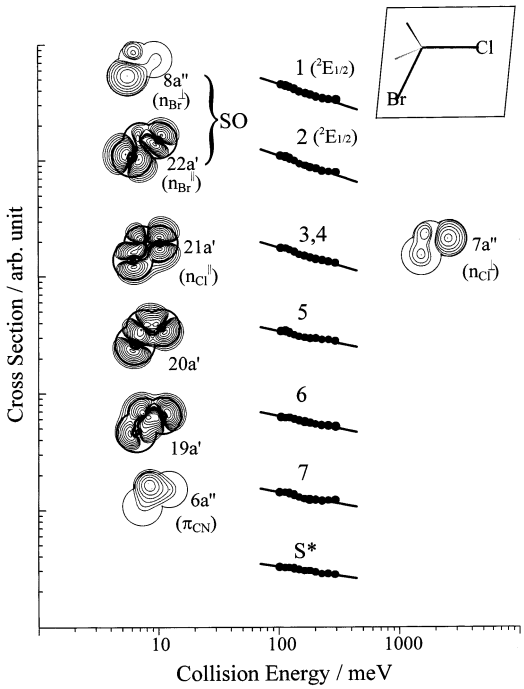

Figure 7. Collision energy dependence of partial ionization cross sections for CH_2BrCl collided by He*(2^3S). Electron density maps of the a′-type orbitals are plotted on the molecular nodal plane; those of the a″-type orbitals are plotted on a plane above 1.7 Å from the nodal plane. SO represents the strong spin−orbit coupling effect.

dissociations ($CH_2BrCl^{**} \rightarrow CH_2 + Cl^{**} + Br^{**}$) may be additional contributions. The increasing background of the PIES (see Figures 1, 2, 4, and 5) also indicates the dissociations occur in the low-electron-energy region. As halogen atoms and a CN group have the large EA values,[24,25] the ionic-pairs such as $He^+Br^-CH_2Cl$ and $He^+CN^-CH_2Br$ may be the intermediates in the reactions. Although no additional bands are observed for these intermediates in this study, the additional bands for the similar intermediates frequently appeared in the PIES.[24,47a−c]

B. CEDPICS and Anisotropic Interactions. In Figures 4−6, the hot spectra are underneath the cold spectra. They indicate that CEDPICS for each band shows the negative slope (see Figures 7−9). However, the distinctly different parameters *m* of these negative slopes are listed in Tables 1−3. As discussed previously,[49] when the entrance channel is governed by a long-range attractive interaction,

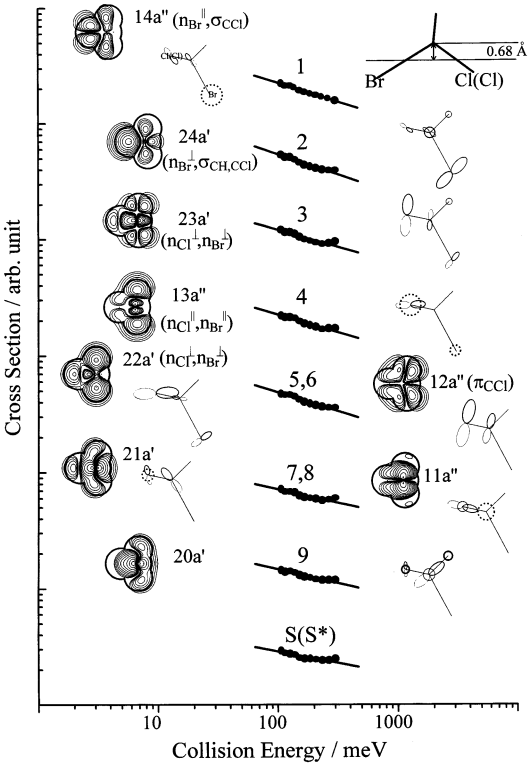

Figure 8. Collision energy dependence of partial ionization cross sections for $CHBrCl_2$ collided by He*(2^3S). Electron density maps are plotted on the plane including the mass center that is 0.68 Å below the carbon atom.

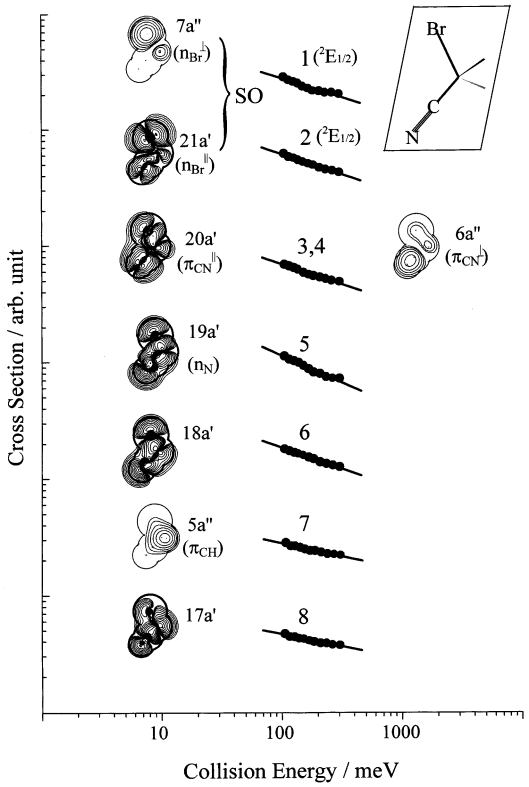

Figure 9. Collision energy dependence of partial ionization cross sections for CH_2BrCN collided by He*(2^3S). Electron density maps of the a′-type orbitals are plotted on the molecular nodal plane; those of the a″-type orbitals are plotted on a plane above 1.7 Å from the nodal plane. SO represents the strong spin−orbit coupling effect.

$$V^*(R) \propto R^{-s} \tag{2}$$

the cross section σ can be expressed by

$$\sigma \propto E_c^{-2/s} \tag{3}$$

where the s value represents the steepness of the attractive potential part of the curve $V^*(R)$. Furthermore, a comparative relationship between experimental CEDPICS and calculated potentials can be established by $m = -2/s$. The s values are estimated to be ca. 5.8 and 4.4, with the m values of bands 1 and 2 for the n_{Br} orbitals, and band 5 for the n_N orbital, respectively, in Tables 1 and 3. These results suggest that the interaction energies for the n_N orbital should decrease more quickly than those for the n_{Br} orbitals and are consistent with the fact that the potential curve E for the n_N orbital damps a little more sharply than the curves B and C for the n_{Br} orbitals (see Figures 10 and 13).

The calculated potential wells can indicate the strength of the attractive interactions. The well depths in the potential curves of the directions perpendicular to the C−Br bond axis in Figures 10a and 13a are much larger (170−200 meV) than those (depth ∼ 100 meV) of the curves F and G in Figure 10b. The wideness of bands 3 and 4 in PIES of Figure 3 can be interpreted by the broad potential wells of the curves D and F in Figure 13b besides the vibrational structures. In particular, the curve D shows a little deeper well than the curve F, which explains well the higher intensity of band 4 with respect to that of band 3 in the PIES of Figure 3. In Table 3, band 5 (19a′, n_N) exhibits the extremely large negative m (−0.46) and ΔE (−290 ± 20 meV) values. Correspondingly, the curve E having a potential well-depth ca. 320 meV in Figure 13b shows that the approaches along or parallel to the CN bond axis are the most attractive. On the basis of the calculated potential curves, the m values obtained from experimental CEDPICS, and the peak shifts ΔE for the n_{Cl}, n_{Br}, n_N, and π_{CN} bands, one can derive the magnitude sequence of the attractive interactions $n_N \gg \pi_{CN} \sim n_{Br} > n_{Cl}$. In Tables 1 and 3, the m values of bands 1 and 2 are almost identical due to the strong SO coupling effects as interpreted above, whereas bands 1 and 2 for $CHBrCl_2$ have different m values in Table 2 because of the strong intramolecular orbital interaction, as discussed in section C.

The interaction anisotropy can be reflected both by the attractive interactions and by the repulsive ones. Bands 5−7 in Table 1 and bands 6−8 in Table 3 show the smaller absolute values of negative m and ΔE, which can be interpreted by the repulsive interactions along C−Cl or C−Br bond axis and around the CH_2 group in Figures 10 and 13. In particular, band 7 (π_{CH}) exhibits the fairly smaller absolute values of m and ΔE ($m = -0.19$, -0.20, and $\Delta E = -10 \pm 40$ meV for CH_2BrCl and CH_2BrCN, respectively). Curve D in Figure 10 correspondingly shows that the approach to the π_{CH} electrons is repulsive.

The steric interaction potentials around $CHBrCl_2$ are a little more complex. In Figure 11, the interaction potential curve on plane *b* is symmetrical, whereas the curve on the plane *a* is significantly asymmetrical. It indicates that the n_{Cl} orbitals interact strongly with the n_{Br} orbital. Furthermore, the curves in Figure 12a indicate that the attractive interactions for the local approaches (A and B) perpendicular to the C−Br bond axis differ from the interactions (B and C) in Figure 10a. The interactions for the local approaches perpendicular to the C−Cl bond axis even show the repulsive characteristics for $CHBrCl_2$ in Figure 12b. In Table 2, the slope parameter of band 1 ($m = -0.32$) differs distinctly from that of band 2 ($m = -0.35$). Because of this fact as well as their different band shapes in Figure 2, it is reasonable to assign bands 1 and 2 with two

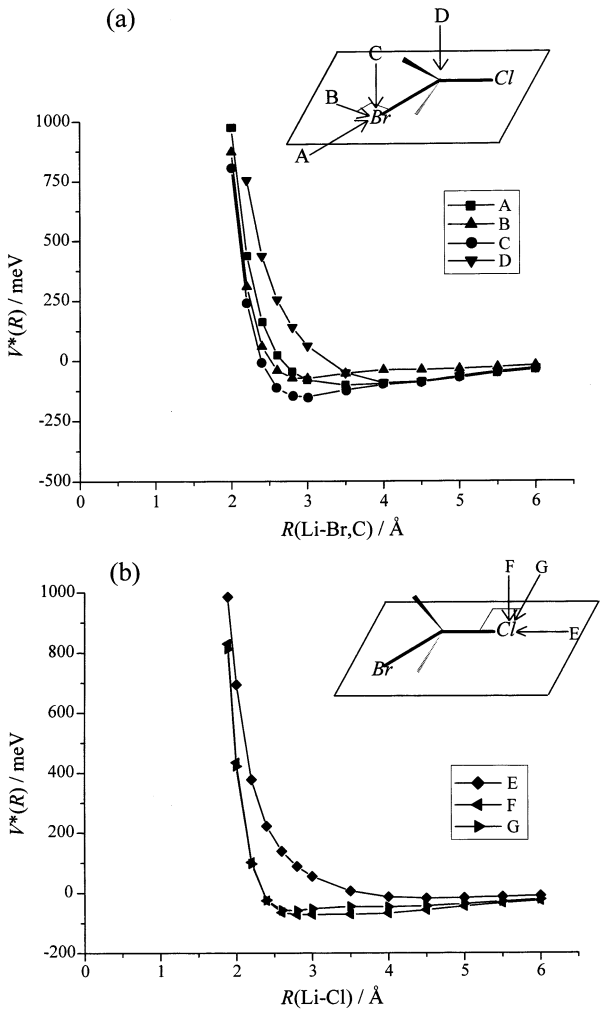

Figure 10. Interaction potential energy curves $V^*(R)$ between Li and the Br, C, or Cl atom in CH_2BrCl. In (a), A is the headon access along the C−Br bond axis, B is the in-plane access perpendicular to the C−Br bond axis, C is the out-of-plane access perpendicular to the C−Br bond axis, and D is the out-of-plane access perpendicular to the carbon atom. In (b), F is the out-of-plane access perpendicular to the C−Cl bond axis, G is the in-plane access perpendicular to the C−Cl bond axis, and E is the head on access along the C−Cl bond axis.

valence-orbital, ionic states rather than the SO split states as given for the other two molecules. Obviously, bands 3 and 4 also have the mixed MO characteristics as given in Table 2 and shown in Figure 8. More details will be presented in section C.

The absolute slope values of CEDPICS for bands S* (autoionization band) and S(S*) are the smallest for each molecule (CH_2BrCl and $CHBrCl_2$). This suggests that the interaction potential around the avoided curve-crossing between He*−CH_2BrCl (or $CHBrCl_2$) should be either repulsive or less attractive than those for the ionizations of the valence orbitals. However, there is no further theoretical or experimental information available. Further investigations on the processes of the collision-excitation followed by dissociations for these systems are needed.

C. Intramolecular Orbital Interactions. For a measurement of the intramolecular orbital (or subunit) interactions, it has been suggested to have a before−after dichotomy of the MOs involved.[50] Under this theoretical frame, Novak et al. proposed a method to calculate this interaction energy between subunits.[30] To study Y → X influence in the molecular pair CH_2X_2 → $CHYX_2$, the interaction energy is equal to the sum of absolute

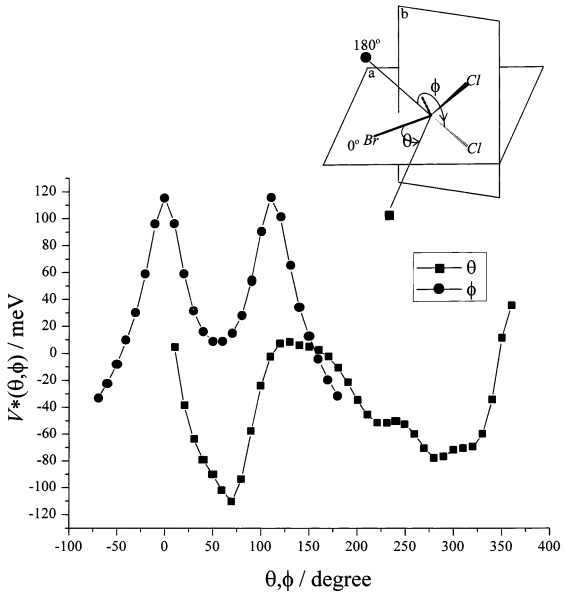

Figure 11. Interaction potential energy curves $V^*(\theta,\phi)$ for Li−$CHBrCl_2$: θ scanning begins from the C−Br bond axis ($\theta = 0°$) with a Li−C distance 4.5 Å; ϕ scanning begins from angle Li−C−Cl (ϕ) = 180° with a Li−C distance 4.5 Å.

values of energy shifts of the four X_2 lone pairs in $CHYX_2$ relative to the energies of the same four lone pairs in CH_2X_2.[30] They estimated that the interaction energies were 0.43 eV for $n_{Cl} \rightarrow n_{Br}$ with a reference of $CH_3Br \rightarrow CH_2BrCl$ and 1.53 eV for $n_{Br} \rightarrow n_{Cl}$ with a reference of $CH_2Cl_2 \rightarrow CHBrCl_2$.[30] With the help of different cases for the same molecules (0.50 eV for $n_{Br} \rightarrow n_{Cl}$ with a reference of CH_3Cl[33] → CH_2BrCl and 0.74 eV for $n_{Cl2} \rightarrow n_{Br}$ with a reference of CH_3Br[33] → $CHBrCl_2$), it follows that intramolecular interactions between halogen atoms in $CHBrCl_2$ are large and lone-pair orbitals have mixed character, as shown in Table 2. Also, the $\pi_{CN} \rightarrow n_{Br}$ interaction energy (1.35 eV) with a reference of CH_3Br[33] → CH_2BrCN is estimated to be larger than $n_{Cl} \rightarrow n_{Br}$ interaction with a reference of $CH_3Br \rightarrow CH_2BrCl$ (0.43 eV).

To study the possibility and magnitude of further splitting of certain bands, one needs investigations on the extent of the orbital interactions by measuring the splitting energies compared to the energies in the absence of such interactions.[50] In this work, we study the orbital $n_{Cl} \leftrightarrow n_{Cl}$, $n_{Cl} \leftrightarrow n_{Br}$, and $n_{Br} \leftrightarrow \pi_{CN}$ interactions on the basis of analyzing their differences of the IP values, electron density distributions, and CEDPICS reflecting anisotropic interactions. First, we should recalculate the splitting energies arising from the $n_{Cl} \leftrightarrow n_{Cl,Br}$ and $n_{Br} \leftrightarrow \pi_{CN}$ interactions. Although the SO coupling effect is not included in the OVGF method,[38] the IP differences of the related MOs can be approximated to be the splitting energies arising from the $n_{Cl} \leftrightarrow n_{Cl,Br}$ and $n_{Br} \leftrightarrow \pi_{CN}$ interactions together with the symmetry lowering effects. In Tables 1 and 3, the splitting energies of the n_{Br} orbitals interacted with the n_{Cl} and π_{CN} orbitals are predicted to be 30 and 70 meV for CH_2BrCl and CH_2BrCN, respectively. Although the splitting energy of the n_{Cl} obritals interacted with the n_{Br} orbitals for CH_2BrCl is predicted to be 70 meV, the split bands (bands 3 and 4) of the n_{Cl} orbitals cannot be resolved due to the low energy resolution. The splitting energies arising from the intramolecular orbital interactions predicted by the OVGF calculations are smaller than the typical SO splitting energies of Br (ca. 300 meV),[41] whereas comparable values to the splitting energy were known for Cl (80 meV). Therefore, it is reasonable to assign bands 1−2 to the SO split states (Figures 1 and 3). In Table 2, the value 240

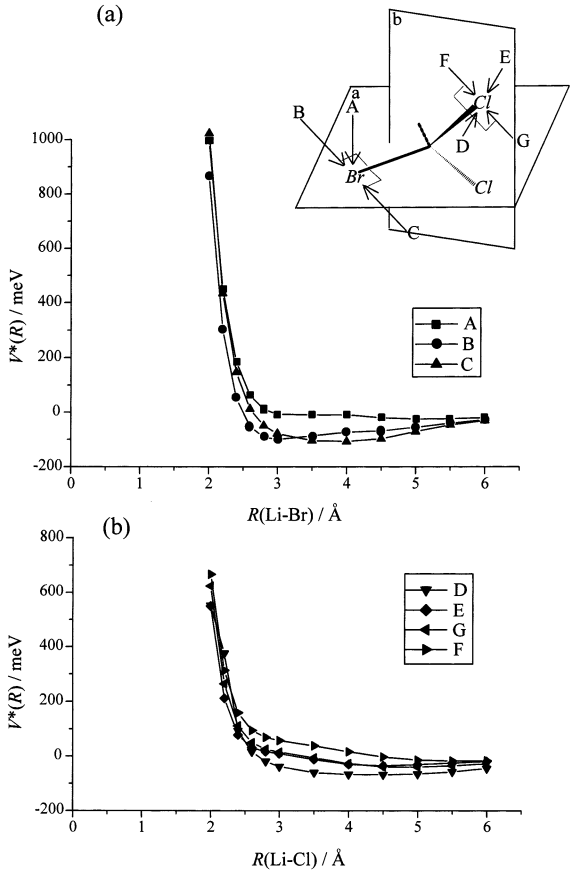

Figure 12. Interaction potential energy curves $V^*(R)$ between Li and the Br or Cl atom in $CHBrCl_2$. In (a), A is the out-of-plane (vertical to the a plane) access perpendicular to the C−Br bond axis, and B and C are the approaches perpendicular to the C−Br bond axis in the a plane. In (b), D and E are the out-of-plane (vertical to the plane b) approaches perpendicular to the C−Cl bond axis, and F and G are the approaches perpendicular to the C−Cl bond axis in the b plane. Here the *a* plane is the H−C−Br plane and the *b* plane is the Cl−C−Cl plane, which is vertical to the *a* plane.

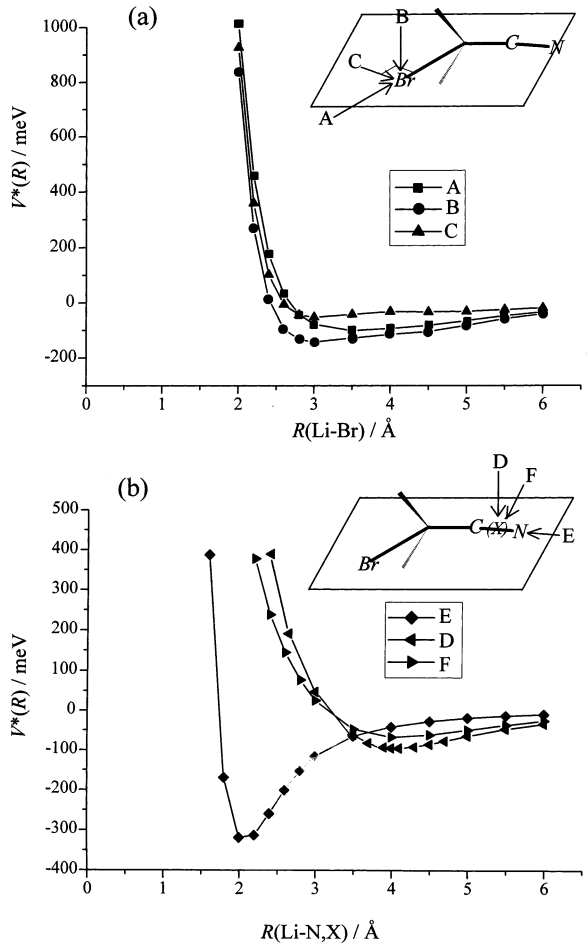

Figure 13. Interaction potential energy curves $V^*(R)$ between Li and the Br, N, or X atom in CH_2BrCN. In (a), A is the headon access along the C−Br bond axis, B is the out-of-plane access perpendicular to the C−Br bond axis, and C is the in-plane access perpendicular to the C−Br bond axis. In (b), D is the out-of-plane access perpendicular to the center point X of the CN bond, F is the in-plane access perpendicular to the center point X of the CN bond C−Cl bond axis, and E is the headon access along the CN bond axis.

meV comparable with the SO splitting energy of n_{Br} orbitals have been predicted for the two lowest IPs of $CHBrCl_2$; therefore, the interactions to the n_{Br} orbitals by four n_{Cl} orbitals are relatively strong with respect to the similar case in CH_2-BrCl. Furthermore, the observed splitting energy (230 meV) between bands 3 and 4 is well predicted by the OVGF calculations (170 meV). These values suggest that the normal ionic states of valence-orbital ionizations should be used for assignments in the electron spectra of $CHBrCl_2$.

It is interesting to study the π_{CN} band splitting by the interactions of the different orbitals in the C_s symmetry molecules. In Figure 14, the IP difference (δIP) between the $\pi_{CN}^{\parallel}$ and $\pi_{CN}^{\perp}$ bands represents the splitting energy observed in the UPS.[13,14,16,33] There are some characteristics in this diagram: the neighboring $\sigma_{CH,CC}$ bonds cannot lead to a significant split of the doubly degenerate π_{CN} orbital in CH_3-CH_2CN and CH_2CHCH_2CN;[13,33] the lone pair orbital of the S atom (n_S) results in the biggest splitting energy (1.85 eV) in CH_3SCN;[14] the calculated $\delta IP(\pi_{CN})$ by the n_{Br} interaction in CH_2BrCN is much smaller than the values for the interactions by the pseudo-π (composed of $\sigma_{CH,CC}$ orbitals of cyclopropane) in cyanocyclopropane (C_3H_5CN)[16,33] and by the $\pi_{C=C}$ in CH_2-CHCN.[13] The hyperconjugation effect leads to another strongly attractive interaction for the He* access perpendicular to the CN bond axis (besides the attractive interaction in the direction of the CN bond axis) for CH_2CHCN,[13] but the n_{Br} orbital of

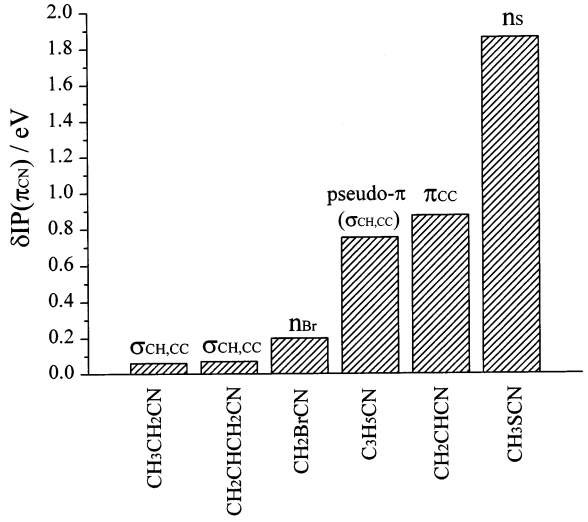

Figure 14. Diagram of the split energy between $\pi_{CN}^{\perp}$ and $\pi_{CN}^{\parallel}$ bands in UPS, by the intramolecular orbital interactions of $\sigma_{CH,CC}$,[12,32] $\sigma_{CH,CC}$(cyclo),[16] n_{Br}, π_{CC},[12,32] and n_S.[14]

CH_2BrCN does not change the characteristics of the interactions around the CN group (see Figure 13), as shown for CH_3CH_2-CN and CH_2CHCH_2CN.[13]

Second, because the electron density maps for each MO shown in Figures 7−9 are delocalized over several atoms, MOs have mixed character. In Figures 7 and 9, the in-plane branch of the n_{Br} orbital ($n_{Br}^{\parallel}$) shows other compositions ($n_{Cl}^{\parallel}$ or $\pi_{CN}^{\parallel}$ electrons) more than the out-of-plane branch $n_{Br}^{\perp}$. By the symmetry, the orbitals having the $n_{Cl}^{\parallel}$ and $n_{Br}^{\parallel}$ characteristics are of the same orbital type (a′), and they are energetically closer than the $n_{Cl}^{\perp}$ and $n_{Br}^{\perp}$ (7a″ and 8a″ for CH_2BrCl), and the $n_{Br}^{\perp}$ and $\pi_{CN}^{\perp}$ (6a″ and 7a″ for CH_2BrCN). Therefore, the intramolecular orbital interactions for the in-plane orbitals are relatively strong. The density maps in Figure 8 show that the 14a″ and 24a′ orbitals have some electron compositions of σ_{CCl}, $n_{Cl}^{\perp}$, and σ_{CH}, and the 23a′−22a′ orbitals have the mixed characteristics of the n_{Cl} and n_{Br} electrons. These indicate that the intramolecular orbital $n_{Cl} \leftrightarrow n_{Cl}$ and $n_{Cl} \leftrightarrow n_{Br}$ interactions in $CHBrCl_2$ are much stronger than those in the other two molecules. In particular, there are two factors to interpret that the intramolecular orbital interactions in $CHBrCl_2$ are stronger than those in CH_2BrCl: the orbital interactions in CH_2Cl_2 are significant[33] and there are double through-space $n_{Cl} \leftrightarrow n_{Br}$ interactions in $CHBrCl_2$ whereas there is only a weak one in CH_2BrCl.

Finally, the orbital interactions are investigated by analyzing the anisotropic interactions and CEDPICS. If bands 1 and 2 correspond to the normal ionic state X^2A'' and A^2A' for CH_2BrCl and CH_2BrCN, the slope parameter of band 1 should distinctly differ from band 2 because curves for two approaches perpendicular to the C−Br bond axis are different in Figures 10a and 13a. However, the parameters are almost equal ($m = -0.35$ and -0.36 for CH_2BrCl, and $m = -0.34$ and -0.35 for CH_2BrCN in Tables 1 and 3). These facts together with the extremely similar interaction potential curve C in Figure 10a and B in Figure 13a indicate the interactions between the n_{Br} orbital and the n_{Cl} or π_{CN} orbital are fairly weak whereas the SO coupling effect of the Br atom is significantly strong. Moreover, as shown in Figure 12, the interaction potentials of the perpendicular approaches to the Cl and Br atoms differ from those of similar approaches in Figures 10 and 13. These results suggest that the lone pair electrons of n_{Cl} or n_{Br} in $CHBrCl_2$ should not be distributed as in CH_2BrCl or CH_2BrCN. The strong intramolecular orbital interactions lead to the MO electrons to be delocalized in $CHBrCl_2$; they also result in the comparable slope parameters for bands 1−6 (see Table 2).

VI. Concluding Remarks

The Penning ionization electron spectra as well as He I ultraviolet photoelectron spectra have been measured for CH_2BrCl, $CHBrCl_2$, and CH_2BrCN. We assign the first bands with the spin−orbit split states in the spectra of CH_2BrCl and CH_2BrCN, whereas the normal valence ionic states are assigned in the spectra of $CHBrCl_2$. Autoionization bands of Rydberg Br** or Cl** atoms are suggested to be produced in the dissociations after excitation transfer from He*(2^3S) metastable atoms to CH_2BrCl and $CHBrCl_2$. On the basis of the observation of the band intensities, band shapes, and CEDPICS and the theoretical calculations of anisotropic interactions, several conclusions can be derived: (1) we rationalize the intramolecular orbital interactions in a strength sequence, $CHBrCl_2$ ($n_{Cl} \leftrightarrow n_{Cl}$, $n_{Cl} \leftrightarrow n_{Br}$) > CH_2BrCN ($\pi_{CN} \leftrightarrow n_{Br}$) ~ CH_2BrCl ($n_{Cl} \leftrightarrow n_{Br}$), and the slightly stronger interactions of the in-plane orbitals with respect to those of the out-of-plane orbitals; (2) the orbital reactivity of Penning ionization is in the strength order $n_N > \pi_{CN} > n_{Br} > n_{Cl}$; (3) both the slopes of CEDPICS and the calculated potential curves indicate that the interaction of an approach along the CN bond axis is the most attractive. The above results support our assignments of the spectra.

Acknowledgment. This work is partially supported by a Grant in Aid for Scientific Research from the Japanese Ministry of Education, Science, and Culture. S.X.T. thanks the Japan Society for the Promotion of Science (JSPS) for a JSPS postdoctoral fellowship (ID No. 00111).

References and Notes

(1) Penning, F. M. *Naturwissenshaften* **1927**, *15*, 818.
(2) Čermák, V. *J. Chem. Phys.* **1966**, *44*, 3781.
(3) Yencha, A. J. In *Electron Spectroscopy: Theory, Technique and Application*; Brundle, C. R., Baker, A. D., Eds.; Academic: New York, 1984; Vol. 5.
(4) Herman, Z.; Čermák, V. *Collect. Czech. Chem. Commun.* **1966**, *31*, 649.
(5) Hotop, H.; Niehaus, A. *Z. Phys.* **1969**, *228*, 68.
(6) Niehaus, A. *Ber. Bunsen-Ges. Phys. Chem.* **1973**, *77*, 632.
(7) (a) Ohno, K.; Mutoh, H.; Harada, Y. *J. Am. Chem. Soc.* **1983**, *105*, 4555. (b) Ohno, K.; Matsumoto, S.; Harada, Y. *J. Chem. Phys.* **1984**, *81*, 4447.
(8) Mitsuke, K.; Takami, T.; Ohno, K. *J. Chem. Phys.* **1989**, *91*, 1618.
(9) Ohno, K.; Takami, T.; Mitsuke, K.; Ishida, T. *J. Chem. Phys.* **1991**, *94*, 2675.
(10) Takami, T.; Mitsuke, K.; Ohno, K. *J. Chem. Phys.* **1991**, *95*, 918.
(11) Dunlavy, D. C.; Martin, D. W.; Siska, P. E. *J. Chem. Phys.* **1990**, *93*, 5347.
(12) Kishimoto, N.; Aizawa, J.; Yamakado, H.; Ohno, K. *J. Phys. Chem. A* **1997**, *101*, 5038.
(13) Ohno, K.; Yamakado, H.; Ogawa, T.; Yamata, T. *J. Chem. Phys.* **1996**, *105*, 7536.
(14) Pasinszki, T.; Yamakado, H.; Ohno, K. *J. Phys. Chem.* **1993**, *97*, 12718.
(15) (a) Pasinszki, T.; Yamakado, H.; Ohno, K. *J. Phys. Chem.* **1995**, *99*, 14678. (b) Ogawa, T.; Ohno, K. *J. Phys. Chem. A* **1999**, *103*, 9925.
(16) Yamakado, H.; Ogawa, T.; Ohno, K. *J. Phys. Chem. A* **1997**, *101*, 3887.
(17) Pasinszki, T.; Kishimoto, N.; Ogawa, T.; Ohno, K. *J. Phys. Chem. A* **1999**, *103*, 7170.
(18) Tokue, I.; Sakai, Y.; Yamasaki, K. *J. Chem. Phys.* **1997**, *106*, 4491.
(19) Imura, K.; Kishimoto, N.; Ohno, K. *J. Phys. Chem. A* **2001**, *105*, 6378.
(20) Imura, K.; Kishimoto, N.; Ohno, K. *J. Phys. Chem. A* **2001**, *105*, 4189.
(21) Tian, S. X.; Kishimoto, N.; Ohno, K. *J. Phys. Chem. A* **2002**, *106*, 6541.
(22) Imura, K.; Kishimoto, N.; Ohno, K. *J. Phys. Chem. A* **2001**, *105*, 6073, 9111.
(23) Tian, S. X.; Kishimoto, N.; Ohno, K. *J. Electron Spectrosc. Relat. Phenom.* **2002**, *125*, 205.
(24) Tian, S. X.; Kishimoto, N.; Ohno, K. *Chem. Phys. Lett.* **2002**, *365*, 40.
(25) Klein, R.; McGinnis, R. P.; Leone, S. R. *Chem. Phys. Lett.* **1983**, *100*, 475.
(26) Pearson, R. G. *Inorg. Chem.* **1988**, *27*, 734.
(27) Brüning, F.; Hahndorf, I.; Stamatovic, A.; Illenberger, E. *J. Phys. Chem.* **1996**, *100*, 19740.
(28) (a) Hacaloglu, J.; Süzer, S. O.; Illenberger, E. *Chem. Phys. Lett.* **1988**, *153*, 268. (b) Heni, M.; Illenberger, E. *Int. J. Mass Spectrum. Ion Processes* **1986**, *153*, 268. (c) van Doren, J. M.; Foley, W. M.; McClellan, J. E.; Miller, T. M.; Kowalak, A. D.; Viggiano, A. A. *Int. J. Mass Spectrum. Ion Processes* **1995**, *149/150*, 423.
(29) (a) Kanda, K.; Yamakita, Y.; Ohno, K. *Chem. Phys. Lett.* **2001**, *349*, 411 and references therein. (b) Yamakita, Y. et al. Private communication. They found that the emission cross sections of the excited CN species produced in the collision between CH_2BrCN and He*(2^3S) atom were extremely weak.
(30) Novak, I.; Li, D. B.; Potts, A. W.; Shareef, A.; Kovac, B. *J. Org. Chem.* **2002**, *67*, 3510.
(31) Novak, I.; Benson, J. M.; Potts, A. W. *Chem. Phys.* **1986**, *107*, 129 and references therein.
(32) Novak, I.; Cvitas, T.; Klasinc, L.; Güsten, H. *J. Chem. Soc., Faraday Trans. II* **1981**, *77*, 2049.
(33) Kimura, K.; Katsumata, S.; Achiba, Y.; Yamazaki, T.; Iwata, S. *Handbook of He I Photoelectron Spectra of Fundamental Organic Molecules*; Japan Scientific: Tokyo, 1981 (see references therein).
(34) Gardner, J. L.; Samson, J. A. R. *J. Electron Spectrosc. Relat. Phenom.* **1976**, *8*, 469.
(35) Pauling, L. *The Nature of the Chemical Bond*; Cornell University: Ithaca, NY, 1960.
(36) (a) von Niessen, W.; Schirmer, J.; Cederbaum, L. S. *Comput. Phys. Rep.* **1984**, *1*, 57. (b) Zakrzewski, V. G.; Ortiz, J. V. *Int. J. Quantum Chem.*

Symp. **1994**, *28*, 23. (c) Zakrzewski, V. G.; Ortiz, J. V. *Int. J. Quantum Chem.* **1995**, *53*, 583.

(37) (a) Rothe, E. W.; Neynaber, R. H.; Trujillo, S. M. *J. Chem. Phys.* **1965**, *42*, 3310. (b) Hotop, H. *Radiat. Res.* **1974**, *59*, 379. (c) Haberland, H.; Lee, Y. T.; Siska, P. E. *Adv. Chem. Phys.* **1981**, *45*, 487.

(38) Frisch, M. J.; Trucks, G. W.; Schlegel, H. B.; Scuseria, G. E.; Robb, M. A.; Cheeseman, J. R.; Zakrzewski, V. G.; Montgomery, J. A., Jr.; Stratmann, R. E.; Burant, J. C.; Dapprich, S.; Millam, J. M.; Daniels, A. D.; Kudin, K. N.; Strain, M. C.; Farkas, O.; Tomasi, J.; Barone, V.; Cossi, M.; Cammi, R.; Mennucci, B.; Pomelli, C.; Adamo, C.; Clifford, S.; Ochterski, J.; Petersson, G. A.; Ayala, P. Y.; Cui, Q.; Morokuma, K.; Malick, D. K.; Rabuck, A. D.; Raghavachari, K.; Foresman, J. B.; Cioslowski, J.; Ortiz, J. V.; Baboul, A. G.; Stefanov, B. B.; Liu, G.; Liashenko, A.; Piskorz, P.; Komaromi, I.; Gomperts, R.; Martin, R. L.; Fox, D. J.; Keith, T.; Al-Laham, M. A.; Peng, C. Y.; Nanayakkara, A.; Gonzalez, C.; Challacombe, M.; Gill, P. M. W.; Johnson, B.; Chen, W.; Wong, M. W.; Andres, J. L.; Gonzalez, C.; Head-Gordon, M.; Replogle, E. S.; Pople, J. A. *GAUSSIAN 98*; Gaussian, Inc.: Pittsburgh, PA, 1998.

(39) Novak, I.; Li, D. B.; Potts, A. W. *J. Phys. Chem. A* **2002**, *106*, 465 and references therein.

(40) Herzberg, G. *Molecular Spectra and Molecular Structure III*; Van Nostrand: Princeton, NJ, 1966; pp 14−19, 337−339.

(41) Eland, J. H. D. *Photoelectron Spectroscopy: An introduction to ultraviolet photoelectron spectroscopy in the gas phase*; Butterworth: London, 1974 (see references therein).

(42) (a) Various saturated halocarbons have been studied by Ohno et al. (unpublished work) in comparisons between He I UPS and He*(2^3S) PIES. For the larger halocarbons, the SO split bands show different shapes in a same spectrum (UPS or PIES), and the higher-electron-energy band is a little stronger than the other in the PIES. (b) Recently, the 2D-PIES of CH_3I has been studied in our group. The slope parameters m of CEDPICS for the SO split bands of the n_I orbital are almost equal ($m = -0.42 \pm 0.02$, -0.42 ± 0.01).

(43) Yamakado, H.; Okamura, K.; Ohshimo, K.; Kishimoto, N.; Ohno, K. *Chem. Lett.* **1997**, 269.

(44) Rozgonyi, T.; Feurer, T.; González, L. *Chem. Phys. Lett.* **2001**, *350*, 155.

(45) (a) McGivern, W. S.; Li, R.; Zuo, P.; North, S. W. *J. Chem. Phys.* **1999**, *111*, 5771. (b) Zuo, P.; McGivern, W. S.; North, S. W. *Phys. Chem. Chem. Phys.* **2000**, *2*, 3785. (c) Lee, S.-H.; Jung, Y.-J.; Jung, K.-H. *Chem. Phys.* **2000**, *260*, 143. (d) Cadman, P.; Simsons, J. P. *Trans Faraday Soc.* **1966**, *62*, 631. (e) Doucet, J.; Gilbert, R.; Sauvageau, P.; Sandorfy, C. *J. Chem. Phys.* **1975**, *62*, 366. (f) Tzeng, W. B.; Lee, Y. R.; Lin, S. M. *Chem. Phys. Lett.* **1994**, *227*, 467. (g) Orkin, V. L.; Khamagonov, V. G.; Guschin, A. G.; Huie, R. E.; Kurylo, M. J. *J. Phys. Chem. A* **1997**, *101*, 174.

(46) Miller, W. H.; Morgner, H. *J. Chem. Phys.* **1977**, *67*, 4923.

(47) (a) Kischlat, W.; Morgner, H. *Z. Phys. A* **1983**, *312*, 305. (b) Beckmann, K.; Leisin, O.; Morgner, H. *Mol. Phys.* **1986**, *59*, 829. (c) Benz, A.; Leisin, O.; Morgner, H.; Seiberle, H.; Stegmaier, J. *Z. Phys. A* **1985**, *320*, 11. (d) Yencha, A. J.; Ganz, J.; Ruf, M.-W.; Hotop, H. *Z. Phys. D* **1989**, *14*, 57. (e) Imura, K.; Kishimoto, N.; Ohno, K. *J. Phys. Chem. A* **2002**, *106*, 3759.

(48) Tian, S. X.; Kishimoto, N.; Ohno, K. *J. Phys. Chem. A* **2003**, *107*, 485.

(49) (a) Illenberger, E.; Niehaus, A. *Z. Phys. B* **1975**, *20*, 33. (b) Niehaus, A. *Adv. Chem. Phys.* **1981**, *45*, 399.

(50) Rabalais, J. W. *Principles of Ultraviolet Photoelectron Spectra*; John Wiley & Sons: New York, 1977.